THE JOURNAL OF PHYSICAL CHEMISTRY A
A JOURNAL OF THE AMERICAN CHEMICAL SOCIETY

pubs.acs.org/JPCA

Article

Exploring Gas-Phase Chemical Reactions in NH_3/B_2H_6 Systems for Chemical Vapor Deposition Using Reactive Molecular Dynamics

Ga-Un Jeong, Adri C. T. van Duin, and Yuan Xuan*

Cite This: J. Phys. Chem. A 2024, 128, 2584−2593

Read Online

ACCESS | Metrics & More | Article Recommendations | Supporting Information

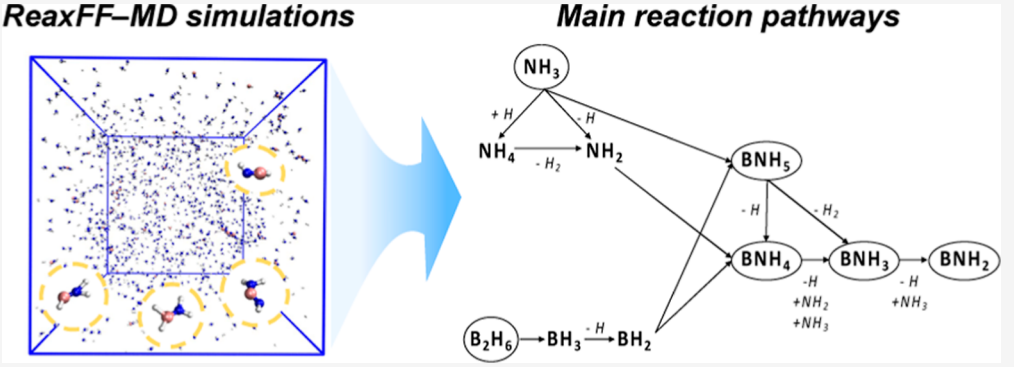

ABSTRACT: Hexagonal boron nitride (hBN) has attracted significant attention as a two-dimensional (2D) material due to its unique structure and properties. In this paper, we investigated the gas-phase reactions between B_2H_6 and NH_3 and the reaction pathways potentially leading to the synthesis of hBN by using ReaxFF-based reactive molecular dynamics (MD) simulations. From the hundreds of chemical reaction pathways observed in these MD simulations, we extracted a highly reduced chemical kinetic model to describe the gas-phase mixture evolution in chemical vapor deposition of hBN using B_2H_6 and NH_3 as precursors. The intent is to integrate this chemical model into future computational fluid dynamics (CFD) simulations of actual hBN deposition testing and production reactors to provide enhanced insights for experimental synthesis processes and reactor optimization. The chemical model of this study will serve as a stepping stone for large-scale simulations.

1. INTRODUCTION

Two-dimensional (2D) hexagonal boron nitride (hBN) is a graphene-like structure formed by the sp^2 hybridized network of boron and nitrogen. hBN is a promising material for electric insulator, heat resistant material, and optical device applications in the deep ultraviolet spectral region because of its chemical and thermal stability, chemical inertness, and good lubricant properties. In addition, the wide band gap of hBN makes it an attractive candidate for semiconductor applications.[1−4]

The chemical vapor deposition (CVD) and metalorganic CVD (MOCVD) methods have been used for large-scale production of hBN with various precursors.[5−11] BF_3/NH_3 and BCl_3/NH_3 have been used to deposit 2D hBN.[12,13] However, their use has been gradually reduced due to the toxicity of boron trifluoride (BF_3) and boron trichloride (BCl_3).[5] Borazine ($B_3N_3H_6$) and ammonia borane ($H_3N_BH_3$) have many advantages because of 1:1 B/N stoichiometry. However, borazine ($B_3N_3H_6$) is an unstable compound and reacts readily to form low volatility polymers. Ammonia borane (H_3NBH_3) is stable under ambient conditions, but its byproduct, monomeric aminoborane (BH_2NH_2), is very active and forms polymeric aminoborane. Therefore, the synthesis of hBN using these sources is relatively complicated.[14−19] Carbon-based precursors such as triethyl boron [$B(C_2H_5)_3$, TEB] and trimethyl boron [$(CH_3)_3B$, TMB] do not have these issues and are widely used for CVD/MOCVD of hBN, but it could lead to carbon contamination in 2D hBN.[10,20−23] In order to circumvent the impurity issues associated with carbon incorporation, the deposition of hBN using diborane (B_2H_6) and ammonia (NH_3) as precursors has been employed.[20,24,25]

It has been found that gas-phase chemical and physical processes play an important role in the deposition rate and quality of hBN. Bansal et al.[26] reported CVD of hBN on C-plane sapphire using B_2H_6 and NH_3 as precursors at high temperatures using two growth modes: continuous mode and flow modulation epitaxy (FME) mode. In continuous mode, precursors are simultaneously introduced into the reactor at

Received: December 8, 2023
Revised: March 12, 2024
Accepted: March 12, 2024
Published: March 26, 2024

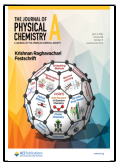

constant flow rates. In the FME mode, precursors are sequentially pulsed into the reactor. It was found that the growth rate increased 25 times when the FME mode was used in comparison to the continuous mode. This was attributed to the decrease in parasitic gas-phase reactions resulting from the sequential introduction of precursors in the FME mode, leading to an increase in the concentration of borazine reaching the substrate surface. However, when a purge step was added between the injection of precursors in FME mode, the formation of borazine was suppressed by reducing the gas-phase mixing, disrupting the deposition of crystalline BN. This study suggests that understanding the interplay between transport processes (mixing) and key gas-phase reactions in the B_2H_6/NH_3 system is essential for improving the rate and quality of hBN deposition.

The gas-phase reactions between B_2H_6 and NH_3 that result in the synthesis of hBN were investigated in earlier research. Murarka et al.[27] noted that while the deposition rate exhibits a weak inverse dependence upon the ammonia concentration, it is linear in the concentration of diborane in the reactant gases. Boron-to-nitrogen ratio in the deposited film falls as the deposition temperature increases and as the $[B_2H_6]/[NH_3]$ in the feed gas drops to low levels. Gomez-Aleixandre et al.[28,29] reported the formation of different intermediate compounds depending on the $[NH_3]/[B_2H_6]$ ratio. When B_2H_6 is in excess, aminodiborane ($B_2H_5NH_2$) is formed. Conversely, in an environment with a high concentration of NH_3, $B_2H_5NH_2$ may interact with other NH_3 molecules to generate various adduct compounds and aminoborane (H_2BNH_2), which then undergoes an additional rearrangement to form borazine ($B_3N_3H_6$, a ring compound). As it is heated further, $B_3N_3H_6$ gradually loses hydrogen until BN is produced. However, the gas-phase chemical reactions leading to these key intermediates are still not well explored, and their rate parameters have not been quantified.

The purpose of this work is to provide a first-principle-based understanding of gas-phase reactions between B_2H_6 and NH_3, necessary for future hBN deposition process optimization. More specifically, we first used ReaxFF-based molecular dynamics (MD) simulations to explore the gas-phase chemistry between B_2H_6 and NH_3. Then, we will identify the reaction pathways that potentially lead to the synthesis of hBN. Finally, we will propose a highly reduced chemical kinetic model extracted from the hundreds of chemical reactions captured in ReaxFF-based MD simulations. The intent is to incorporate this chemical model in future computational fluid dynamics (CFD) simulations of actual hBN deposition testing (e.g., Bansal's experiments[26]) and production reactors. Such large-scale CFD simulations are expected to provide enhanced insights for experimental synthesis processes and reactor optimization.[30]

2. METHODOLOGY

The ReaxFF-based MD methodology is used for reaction exploration to enable longer simulation time with many more reaction events compared to quantum chemical calculations.

2.1. ReaxFF. ReaxFF is a bond-order-based force field with instantaneous connectivity for chemical bonds, depending on the atomic local environment. The bond order is calculated directly from an interatomic distance and is updated at every iteration, which captures bond formation and breaking. The total energy of a system consists of many-body empirical potential terms. There are bond-order-dependent energy terms such as bond, angle, and torsion and nonbonded interaction terms such as van der Waals and Coulomb interactions. The ReaxFF method uses the Morse potential for the van der Waals interactions to properly describe the short-range interactions and uses the electronegativity equalization method (EEM) for Coulomb interactions to calculate atomic charges. ReaxFF calculates the energy of each atom in the system using the following equation

$$E_{system} = E_{bond} + E_{over} + E_{under} + E_{lp} + E_{val} + E_{tor} + E_{vdWaals} + E_{Coulomb}$$

where E_{bond} (bond energy), E_{over} (over-coordination penalty energy), E_{under} (under-coordination penalty energy), E_{lp} (lone pair energy), E_{val} (valence angle energy), and E_{tor} (torsion angle energy) are bond-order-dependent terms. $E_{vdWaals}$ (van der Waals energy) and $E_{Coulomb}$ (Coulomb energy) are nonbonded terms. More details about the ReaxFF energy descriptions are given in previous publications.[31−33]

2.2. ReaxFF Molecular Dynamics Simulation Details. ReaxFF MD simulations of NH_3/B_2H_6 were performed in 3D-periodic boxes with a fixed density of 0.02 g/mL over 4 different temperatures: 2000, 2500, 3000, and 3500 K. In all simulations, 1000 NH_3 molecules and 40 B_2H_6 molecules were placed in the simulation box with a NH_3/B_2H_6 ratio of 25:1, much lower than the 2000:1 used in Bansal's experiment. The relatively high temperature range, high mixture density, and low NH_3/B_2H_6 ratio are selected so that enough reaction events occur within a reasonable amount of computational time, which has already been verified by Lele et al.[34]

For each simulation, the NH_3 and B_2H_6 molecular structures consisting of the initial simulation configuration were energy minimized at 0 K. These optimized structures were randomly placed in a 3D-periodic box of an appropriate size to reach the desired density of 0.02 g/mL. Then, the system was equilibrated at 300 K under *NVT* ensemble, using Berendsen thermostat with a temperature damping constant of 100 fs. This step was run so that the randomly arranged molecules could be stabilized without any chemical reaction occurring. Following the equilibration, *NVT* simulations were performed at the desired temperatures for 1 ns with a time step of 0.1 fs. For each temperature, we performed 3 statistically independent simulations with three different initial configurations for ensemble averaging to reduce statistical noise. All the results reported in this work were based on ensemble-averaged data from the three *NVT*-MD simulations. All ReaxFF simulations were performed using the previously developed and validated B/N/H force field.[34] We identified all reactions that occurred during MD simulations at every temperature by using an in-house reaction analysis code. This code operates on the assumption that a reaction event occurs when a species with a different chemical formula is identified. Such reaction events are identified across all simulations, and their occurrence is given as the difference between the forward and backward reactions, and then averaged over the number of simulations at a given temperature.[34−36] Snapshots of the initial and final simulation configurations are shown in Figure 1.

3. RESULTS AND DISCUSSION

3.1. Chemical Reaction Pathway Analysis. Major products and dominant reaction pathways were identified from ensemble-averaged ReaxFF simulation results at all 4 temperatures.

https://doi.org/10.1021/acs.jpca.3c08051
J. Phys. Chem. A 2024, 128, 2584−2593

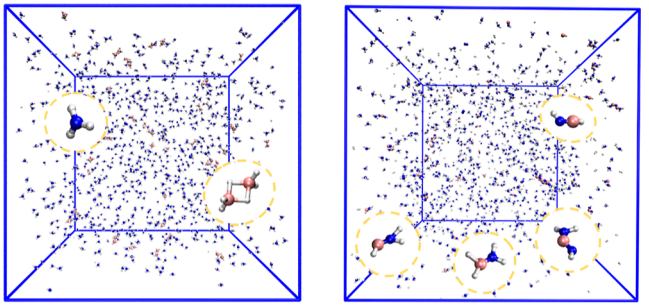

Figure 1. Snapshots of simulations of (a) initial and (b) final configurations. The blue, pink, and white spheres indicate nitrogen, boron, and hydrogen, respectively. Key reactant and product molecules are magnified in these snapshots.

3.1.1. Identification of Major Intermediates and Radicals. We examined the ReaxFF-based MD simulation results across all 4 temperatures and identified major intermediate species and key radicals. Figure 2 shows the temporal evolution of reactants (NH_3 and B_2H_6), some major intermediate products (BNH_4, BNH_3, and BNH_2), and radicals (NH_4, NH_2, BH_3, and BH_2) observed at all 4 temperatures. Because of the large number of NH_3 in the system, the number of NH_3 consumed was plotted, instead of the number of NH_3 molecules.

As shown in this figure, B_2H_6 was observed to dissociate to BH_3 rapidly at all of the temperatures. As expected, this dissociation becomes faster with increasing temperature. The consumption of the other reactant, NH_3, on the other hand, was found to be much slower. This is also expected because the N−H bond in NH_3 is much stronger as the B−H bonds in B_2H_6.

The formation of NH_4, NH_2, and BH_2 was observed following the consumption of the reactants, which also generated H radicals and H_2. With the help of NH_2 and BH_2 radicals, BN intermediate species such as BNH_5, BNH_4, and BNH_3 are formed. These intermediate species led to the formation of BNH_2 which was found in large amounts toward the end of the simulations above 2500 K (Figure 2b−d). These compounds were also observed at lower temperatures (Figure 2a) but in smaller amounts. Radicals such as H and BNH_5, which are produced and consumed very rapidly, are not shown in Figure 2. The large amount of BNH_2 formed toward the end of the ReaxFF simulations under excess NH_3 conditions is in good agreement with previous studies.[28,29] This compound is thermodynamically stable and serves as a building block for the formation of borazine ($B_3N_3H_6$), which leads to hBN formation by gradual dehydrogenation. For these reasons, BNH_2 is considered the end compound in our subsequent chemical kinetic analysis. This BNH_2 gradually grows into a larger boron−nitrogen species in the gas phase. As shown in

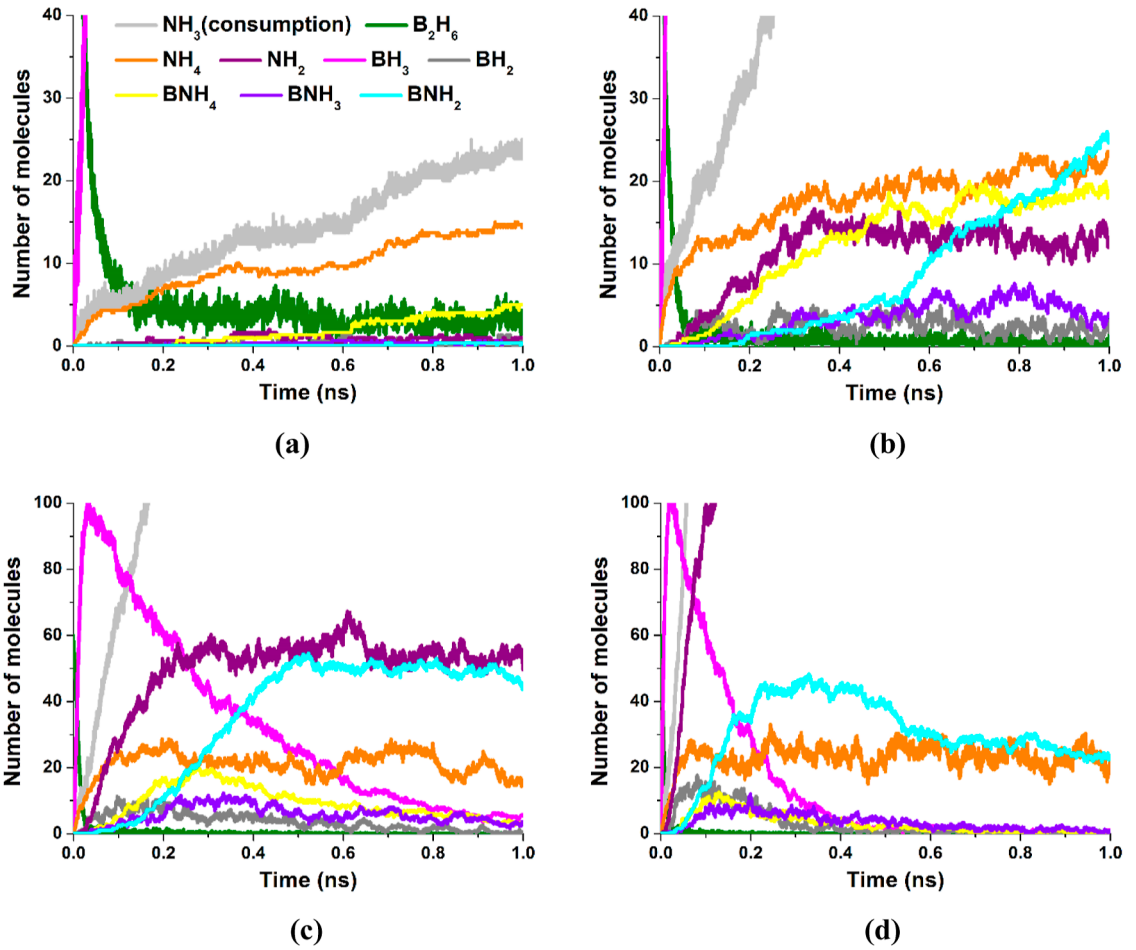

Figure 2. Temporal evolution of the reactants, major intermediate products, and radicals observed during ReaxFF simulations at (a) 2000, (b) 2500, (c) 3000, and (d) 3500 K.

https://doi.org/10.1021/acs.jpca.3c08051
J. Phys. Chem. A 2024, 128, 2584−2593

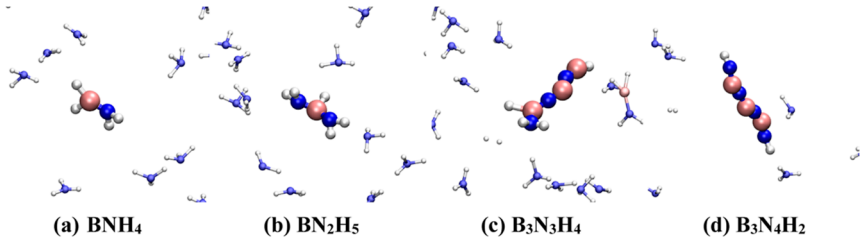

Figure 3. Highest molecular weight B−N species observed in the (a) 2000, (b) 2500, (c) 3000, and (d) 3500 K ReaxFF MD simulations, respectively.

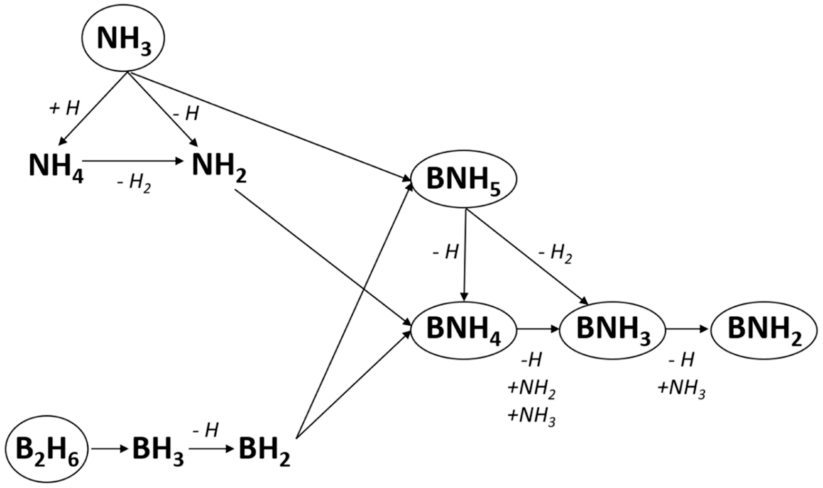

Figure 4. Summary of the main reaction pathways with the major species from the initial precursors B_2H_6 and NH_3 to the end species BNH_2.

Figure 3, we observed B−N species with a higher molecular weight at the end of the simulations (1 ns). Although they are all straight chains, it is expected that ring formation will occur in longer simulations.

3.1.2. Identification of Major Chemical Reaction Pathways. We examined all of the reactions occurring in the ReaxFF simulations and ranked them according to their number of occurrences. Overall, 1581 elemental reactions (four temperatures combined) were discovered, but most of these reactions were found to occur at low frequency. The major reactions from the reactants to the most thermodynamically stable B−N-containing products (identified in Section 3.1.1) are summarized in Figure 4.

When B_2H_6 is consumed, it splits into two BH_3 by unimolecular decomposition and undergoes dehydrogenation producing BH_2, which makes BH_2 highly temperature sensitive. NH_3 primarily leads to NH_2 and NH_4. NH_2 can be produced from NH_3 in two ways. The "$NH_3 + H \rightarrow NH_4 \rightarrow NH_2 + H_2$" path is dominant at low temperatures, whereas the "$NH_3 + NH_3 \rightarrow NH_4 + NH_2$" reaction is dominant at high temperatures. This is because the N−H bonds in NH_3 have large bond dissociation energies and need high temperatures for bond breaking. In contrast, the production of NH_4 from NH_3 involves hydrogen addition with a low energy barrier, which makes it the preferred pathway at low temperatures. This explains why NH_2 is largely unaffected by the temperature. Subsequently, NH_2 will combine with BH_2 to form the first thermodynamically stable BN compound, BNH_4. It can also be formed from its radical BNH_5, produced from the NH_3 and BH_2 combination. BNH_4 then goes through several dehydrogenation reactions to eventually form the end thermodynamically stable BN compound detected in the ReaxFF simulations, BNH_2. All of these BN species exhibit high temperature sensitivity. Many reactions involved in their formation, as stated above, are strongly temperature-dependent.

3.2. Chemical Model Extraction. An accurate and concise chemical kinetic model to describe the gas-phase reactions in B_2H_6/NH_3 systems was extracted from the ReaxFF simulation results. Such chemical models are a critical input to the CFD simulations that can predict hBN deposition to enable deposition chamber design and optimization.

3.2.1. Pathway Selection. CFD simulations with chemical reactions are generally computationally expensive due to the high computational cost associated with chemical reaction rate evaluation and time integration. Therefore, from ReaxFF simulations, we extracted only a highly reduced set of reactions covering the major pathways with major intermediates and key radicals to represent the thousands of detailed elemental reactions discovered in the MD simulations. It includes all reactions with the highest production and consumption rates of the major intermediate species at all temperatures. We ensured that at least 70% of the total production and consumption rates of the major compounds were accounted for by the reduced set of reactions. Table 1 lists all selected reactions from reactant dissociation to the formation of the last thermodynamically stable molecule, BNH_2.

3.2.2. Reaction Lumping and Rate Determination. In order to ensure that the reduced set of reactions can accurately reproduce the time histories of major compounds formed in ReaxFF MD simulations, it is necessary to lump some of the unconsidered, missing reactions from ReaxFF simulations into the selected reactions that are similar by adding their number of occurrences to that of the corresponding major reactions. As

https://doi.org/10.1021/acs.jpca.3c08051
J. Phys. Chem. A 2024, 128, 2584−2593

Table 1. Extracted Main Reactions with Fitted Arrhenius Parameters

reaction	E_a (kcal/mol)	A
$B_2H_6 \rightarrow BH_3 + BH_3$	0.67065	2.03134×10^{11}
$NH_3+BH_2 \rightarrow BNH_5$	1.95447	1.61757×10^{13}
$NH_4 \rightarrow NH_2 + H_2$	62.68034	3.30220×10^{14}
$NH_3 + BH_3 \rightarrow NH_4 + BH_2$	29.20948	2.22712×10^{13}
$NH_3 + H \rightarrow NH_2 + H_2$	−5.11268	1.52225×10^{12}
$BH_3 \rightarrow BH_2 + H$	46.67474	2.63361×10^{12}
$BH_3 + H \rightarrow BH_2 + H_2$	−5.34185	4.96490×10^{13}
$BH_3 + NH_2 \rightarrow BH_2 + NH_3$	14.58318	1.65079×10^{14}
$NH_3 + NH_3 \rightarrow NH_4 + NH_2$	54.52575	1.12763×10^{14}
$BNH_3 + NH_3 \rightarrow BNH_2 + NH_4$	12.14728	3.40966×10^{13}
$BNH_4 + NH_3 \rightarrow BNH_3 + NH_4$	13.88708	2.16079×10^{12}
$BNH_5 \rightarrow BNH_4 + H$	6.42715	1.28090×10^{11}
$BH_2 + NH_2 \rightarrow BNH_4$	326.61463	3.79662×10^{36}
$BNH_5 \rightarrow BNH_3 + H_2$	11.77157	1.0415×10^{11}
$NH_2 + BNH_4 \rightarrow NH_3 + BNH_3$	−19.39510	1.32575×10^{12}
$BNH_4 \rightarrow BNH_3 + H$	242.47318	1.00891×10^{26}
$BNH_3 \rightarrow BNH_2 + H$	53.23173	1.30655×10^{13}
$NH_2 + BNH_2 \rightarrow BN_2H_3 + H$	−3.07190	9.79604×10^{12}

such, this lumping process allows the production and consumption rates of major species calculated from only the main reactions (Table 1) to be comparable to those calculated from ReaxFF simulations.

Minor reactions with reactants coming from the same origin as those of a major reaction were lumped into that major reaction. For instance, the minor reaction "$BN_2H_6 \rightarrow BNH_2 + NH_4$" was lumped into the major reaction "$BNH_3 + NH_3 \rightarrow BNH_2 + NH_4$", since the reactant BN_2H_6 was mainly formed from $BNH_3 + NH_3$; the reaction "$B_2H_5 \rightarrow BH_3 + BH_2$" was lumped into the major reaction "$B_2H_6 \rightarrow BH_3 + BH_3$" because B_2H_5 is mainly formed by H-abstraction from B_2H_6. However, minor reactions with reactants formed too late than those of a major reaction were not lumped into the major reaction, even if these reactants came from the same origin. For example, the minor reaction "$B_4H_{11} \rightarrow B_2H_5 + BH_3 + BH_3$" was not lumped into the major reaction "$B_2H_6 \rightarrow BH_3 + BH_3$", even though B_4H_{11} was mainly produced by B_2H_6 recombination followed by H-abstraction. This was because B_4H_{11} was only formed toward the end of the simulations, whereas B_2H_6 decomposition to BH_3 was observed to occur only during the early stage of the simulations (within the first 0.1 ns).

After reaction lumping, the effective reaction rates of all major reactions, k, were calculated for all four temperatures. The rate constant was calculated based on the same methodology as proposed by M. Döntgen et al.[37] to analyze a large number of reactions from a single reactive MD simulation and derive kinetic parameters of the reactions.

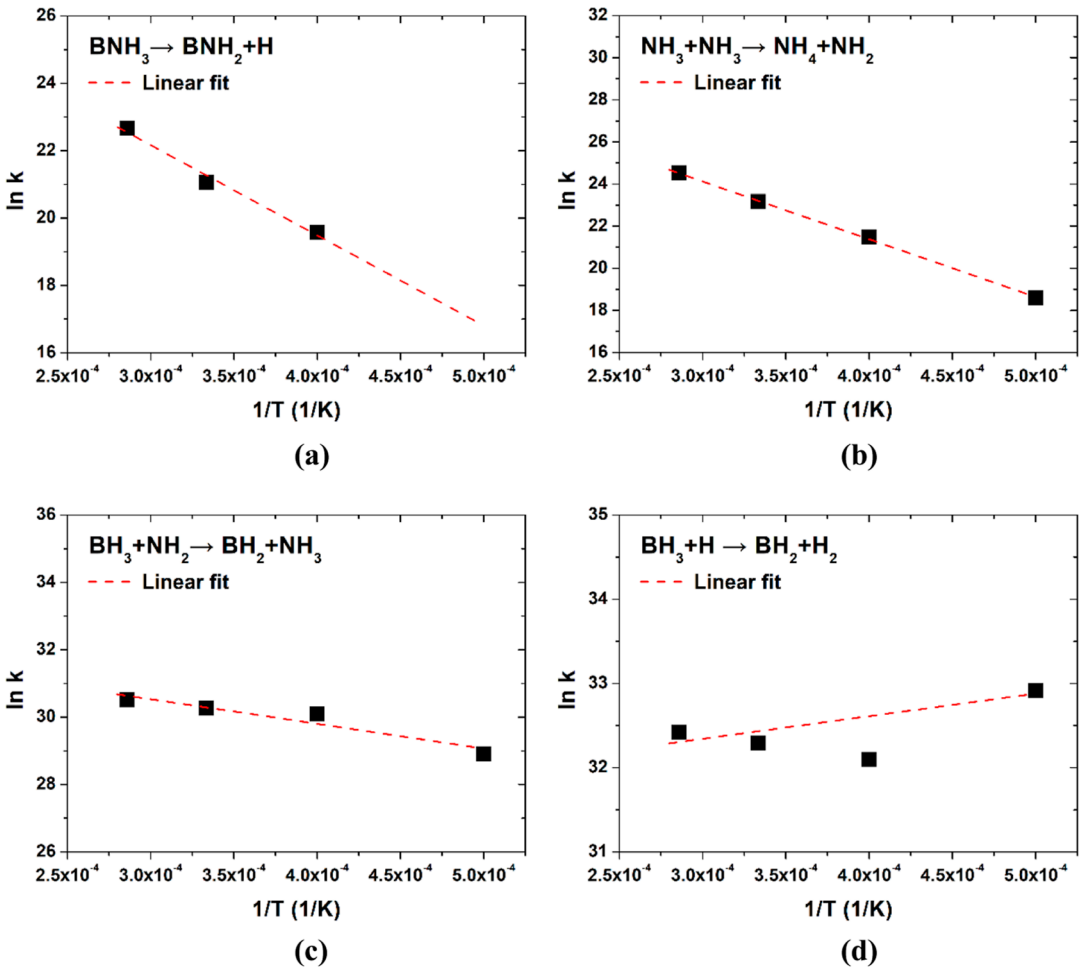

Figure 5. Logarithm of the rate constants $[\ln(k)]$ as a function of the inverse of temperature $(1/T)$ for (a,b) high temperature reactions and (c,d) low temperature reactions.

https://doi.org/10.1021/acs.jpca.3c08051
J. Phys. Chem. A 2024, 128, 2584−2593

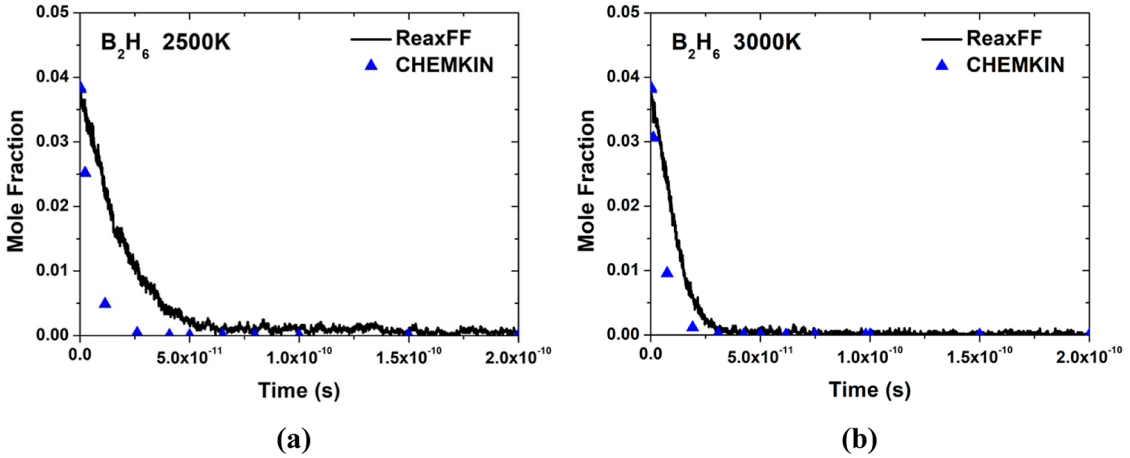

Figure 6. Comparisons of time histories of B_2H_6 predicted from ReaxFF simulations and CHEMKIN simulations with the extracted chemical model at (a) 2500 and (b) 3000 K.

Figure 5 shows the logarithm of the reaction rates obtained from ReaxFF as a function of the inverse of temperature for 4 representative reactions. The rate constants of reactions (a) and (b) were found to be highly temperature-dependent, since they have stable molecules as reactants which require high temperatures to break the bonds; whereas the rate constants of reactions (c) and (d) show weak dependence on temperature, since their reactants are radicals highly reactive at all temperatures. More importantly, the clear linear dependence of $\ln(k)$ on $1/T$ observed for almost all reactions strongly suggests that the Arrhenius law

$$k = A \exp\left(-\frac{E_a}{RT}\right)$$

can be used to accurately describe the temperature dependence of the reaction rates. In the Arrhenius equation above, A is the pre-exponential factor, E_a is the activation energy, and R is the ideal gas constant. Note that the rate constant for reaction (a) is missing at the lowest temperature. This is because this reaction did not occur in the ReaxFF simulations at such a low temperature. The temperature dependence of the rate constants of all other reactions listed in Table 1 is quantified in Figure S1 in the Appendix.

The $\ln(k) \sim 1/T$ data is linearly fitted for all reactions listed in Table 1 to obtain the Arrhenius parameters (A and E_a), as shown in Figure 5 for the 4 representative reactions and in Figure S1 in the Appendix for all other selected reactions. The obtained Arrhenius parameters are listed in Table 1 for all reactions selected. It is shown that the Arrhenius equation fitting is appropriate for almost all reactions with high root-mean-square (R^2) values. For unimolecular decomposition or bimolecular reactions between 2 stable molecules, large pre-exponential factors and high activation energies were obtained from the fitting, as shown, for instance, for the reactions "$BNH_3 \rightarrow BNH_2 + H$" and "$NH_3 + NH_3 \rightarrow NH_4 + NH_2$" in Figure 5a,b. This is consistent with the high collision frequencies between the reactants and high temperatures required to break the strong bonds in the reactants. These reactions are typically dominant at high temperatures. On the other hand, for reactions involving radicals, small pre-exponential factors and low activation energies were obtained from the fitting, as shown, for instance, for the reactions "$BH_3 + NH_2 \rightarrow BH_2 + NH_3$" and "$BH_3 + H \rightarrow BH_2 + H_2$" in Figure 5c,d. This is consistent with the low collision frequencies with radicals and their high reactivity, which typically requires low energy barriers. These reactions are typically more dominant at low temperatures. As shown in Table 1, the reactions selected in our reduced chemical model include all types of reactions described above. Therefore, our chemical model is expected to be applicable and accurate over a wide temperature range.

3.3. Chemical Model Validation. In this section, we validate the highly reduced chemical kinetic model extracted from ReaxFF simulations (Section 3.2) by comparing species time histories predicted by this model with ReaxFF results under the same conditions.

3.3.1. Validation Configurations in CHEMKIN. Continuum-scale chemical kinetic simulations using the extracted gas-phase chemical model were set up under the same conditions as those used in the ReaxFF simulation (Section 2.2) for all 4 temperatures (2000, 2500, 3000, and 3500 K). These simulations were performed using CHEMKIN, a widely used chemical kinetics simulator that models idealized reacting flows.[38] To mimic the ReaxFF simulations, a closed 0D homogeneous batch reactor model was selected in CHEMKIN because there are no effects of convection or diffusion, and species evolutions are governed by chemical reactions in the ReaxFF simulations. To be consistent with the ReaxFF simulation conditions, at each temperature, the NH_3 and B_2H_6 precursors were prescribed to have initial mass fractions of 0.96154 and 0.03846, respectively (a molecule number ratio of 25:1), and constant temperature, pressure, and volume were maintained throughout the simulation to keep a constant density of 0.02 g/mL. The CHEMKIN simulation was carried out for 5 ns at each temperature.

CHEMKIN simulations typically require three input data: a chemical kinetic model with Arrhenius rate parameters, thermodynamic properties for all species involved (e.g., specific heats, enthalpies, and entropies), and transport properties (e.g., viscosity and diffusivity). However, given that we used the 0D homogeneous reactor configuration with a constant temperature in the CHEMKIN simulations, we did not need to provide any thermodynamic or transport property data. Only the reaction pathways and their chemical kinetic parameters extracted from ReaxFF (Table 1) were provided as input for CHEMKIN (Table S1).

3.3.2. Comparisons between ReaxFF and CHEMKIN Results. Comparisons of the time evolutions of B_2H_6, NH_3,

https://doi.org/10.1021/acs.jpca.3c08051
J. Phys. Chem. A 2024, 128, 2584−2593

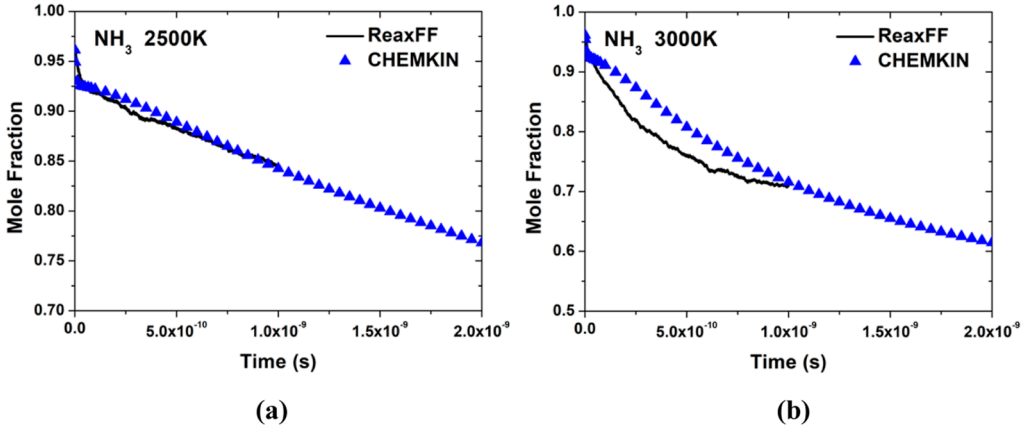

Figure 7. Comparisons of time histories of NH_3 predicted from ReaxFF simulations and CHEMKIN simulations with the extracted chemical model at (a) 2500 and (b) 3000 K.

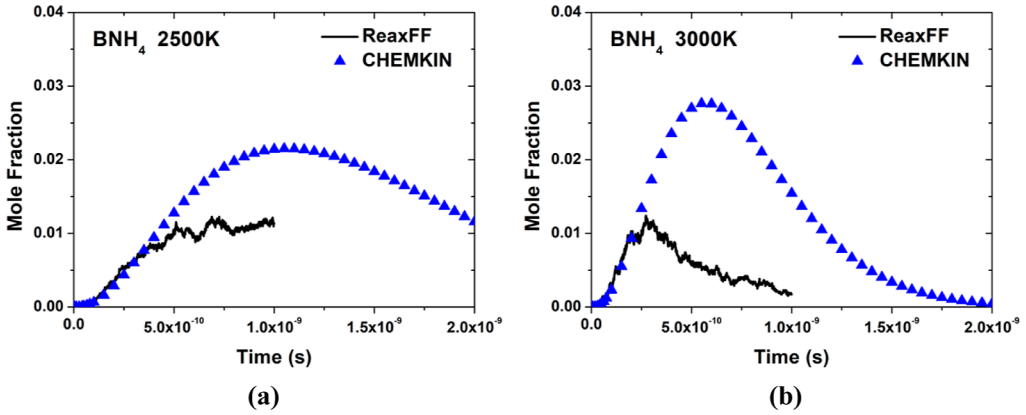

Figure 8. Comparisons of time histories of BNH_4 predicted from ReaxFF simulations and CHEMKIN simulations with the extracted chemical model at (a) 2500 and (b) 3000 K.

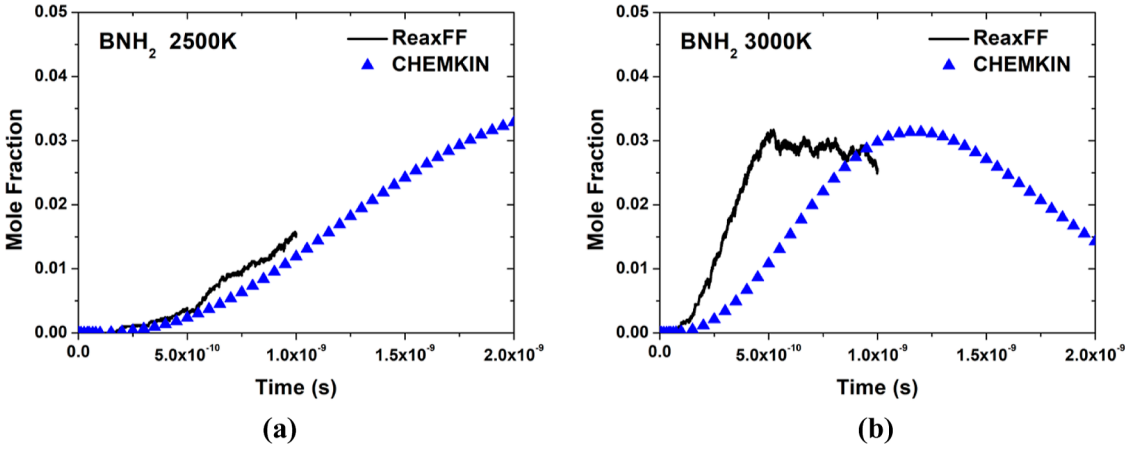

Figure 9. Comparisons of time histories of BNH_2 predicted from ReaxFF simulations and CHEMKIN simulations with the extracted chemical model at (a) 2500 and (b) 3000 K.

BNH_4, and BNH_2 between ReaxFF and CHEMKIN simulations are shown in Figures 6–9 for 2 temperatures, 2500 and 3000 K. Comparisons for other species at the other 2 temperatures are shown in Figure S2 in the Appendix. Overall, it can be observed that the CHEMKIN predictions using the extracted chemical kinetic model are in reasonable agreement with the ReaxFF results, especially for stable molecules (mole fraction differences within a factor of 2). For radicals that are typically rapidly produced and consumed, the agreement is typically within a factor of 3, partly due to the higher levels of statistical uncertainties embedded in ReaxFF results. Considering that the set of chemical reactions in the chemical model is highly reduced compared to the hundreds of reactions observed in ReaxFF simulations, discrepancies with ReaxFF results are inevitable. All errors that occur at each stage of building a downsized chemical model, such as major reaction

https://doi.org/10.1021/acs.jpca.3c08051
J. Phys. Chem. A 2024, 128, 2584−2593

selection, lumping, and Arrhenius fitting, accumulate for any compound, especially the late-forming compounds. Nevertheless, the performance of this extracted chemical model is comparable to that of some well-established, extensively validated chemical models in the literature for reacting systems with well-known chemistry, for instance, the GRI-3.0 model for methane combustion and the Glarborg model for NH_3 oxidation.[39,40]

Figure 6 compares the ReaxFF and CHEMKIN simulation results for the time evolution of B_2H_6, the deficient initial precursor. It is observed that both the extracted chemical model and ReaxFF predict a similar level of temperature dependence of the B_2H_6 decomposition rate (moderate increase in the rate with increasing temperature). Our chemical model predicts a slightly faster B_2H_6 decomposition, mainly through $B_2H_6 \rightarrow BH_3 + BH_3$, leading to an earlier onset of radical product BH_3. The overprediction of the B_2H_6 decomposition rate is improved at higher temperatures (e.g., 3000 K vs 2500 K). This overprediction can be attributed to the uncertainties in the statistics collected in ReaxFF simulations, in the Arrhenius fitting, and in the reaction lumping process, where other B_2H_6 decomposition and BH_3 formation reactions occurring at slightly later stages were lumped into $B_2H_6 \rightarrow BH_3 + BH_3$.

Figure 7 compares the ReaxFF and CHEMKIN simulation results for the time evolution of NH_3, the initial precursor of NH_3, in abundance. It is observed that both the extracted chemical model and ReaxFF predict a strong dependence of the NH_3 consumption rate on the temperature, with much higher rates at higher temperatures. This is consistent with the high activation energies associated with almost all of the NH_3 consumption reactions. The good agreement between ReaxFF and CHEMKIN predicted NH_3 time histories suggests that nitrogen flux from NH_3 to its associated radicals (NH_2 and NH_4) is well predicted by the extracted chemical model. This is crucial for the accurate prediction of the formation of B−N compounds since the conversion from NH_3 to its radicals is the rate-limiting step (slow reactions compared to the rapid B_2H_6 decomposition reactions), leading to the first B−N-containing species. Therefore, the overpredicted B_2H_6 decomposition by the extracted chemical model, as stated above, does not affect the onset of B−N compounds, such as BNH_4.

Figure 8 compares the ReaxFF and CHEMKIN simulation results for the time evolution of BNH_4, the first stable B−N-containing molecule formed primarily from the combination of NH_2 and BH_3 radicals. It is observed that the onset and initial production of this species are predicted very well by the chemical model at all temperatures. However, its consumption rate is underpredicted, which leads to an overprediction of its peak mole fraction in the CHEMKIN simulations. This can be attributed to the uncertainties in the Arrhenius fitting of BNH_4 consumption reactions. In addition, in the ReaxFF simulations, some B−N compounds go through aggregation reactions to form relatively large B−N clusters ($B > 10$, $N > 10$). Such reactions were not considered in the extracted chemical kinetic model, which could also lead to an underprediction of BNH_4 consumption in the CHEMKIN simulations.

Figure 9 compares the ReaxFF and CHEMKIN simulation results for the time evolution of BNH_2, which is considered the end thermodynamically stable compound identified in the gas phase (large B−N clusters excluded) from ReaxFF simulations. Due to the delayed consumption of BNH_4 predicted by our chemical kinetic model, the formation of BNH_2 is also slightly delayed compared to ReaxFF results. This is because BNH_2 is formed from BNH_4 via BNH_3 by dehydrogenation. As we discussed earlier, late-forming compounds have cumulative errors across all reactions involved in reaching these species, resulting in more discrepancies with ReaxFF-MD simulations. Despite this, the rates of increase in BNH_2 mole fraction are similar between ReaxFF and CHEMKIN simulations at all temperatures considered. This suggests that the production rates of BNH_2 are well-reproduced by our chemical model compared to ReaxFF. As detailed in a previous experimental study,[28] BNH_2 serves as the building block for borazine ($B_3N_3H_6$) formation, which leads to hBN surface deposition. Another previous study using a computational approach[41] also found that HBNH and $B_3N_3H_6$ are the most effective precursors for producing BN nanostructures, especially 2D planar structures such as hBN. They also studied synthetic products across a range of temperatures and reported that 2000 K is the most productive temperature, achieving the optimal balance between promoting hBN network formation and preventing the formation of nonreactive N_2. At lower temperature (1500 K), the products have small flakes and amorphous structures, while at higher temperature (2500 K), the products have amorphous turbostratic *t*-BN-structures. Therefore, the accurate prediction of BNH_2 by our chemical model is expected to lead to promising hBN surface deposition rate predictions when this model is combined with an hBN surface chemistry model and applied in CFD simulations of large-scale CVD devices for hBN production.

4. CONCLUSIONS

In this study, we investigated the gas-phase reactions between B_2H_6 and NH_3 and the reaction pathways potentially leading to the synthesis of hBN by using ReaxFF-based reactive MD simulations. We identified major intermediate species, radicals, and B−N-containing compounds, as well as main reaction pathways dominant at high and low temperatures. A highly reduced chemical kinetic model was extracted from ReaxFF simulations. We incorporated reactions dominant at high and low temperatures and lumped unconsidered reactions into the selected reactions to achieve high accuracy and high applicability across a wide range of temperatures. We obtained the reaction rate parameters for the selected reactions using Arrhenius fitting and validated the chemical model in CHEMKIN against ReaxFF simulation results.

The extracted chemical kinetic model for NH_3/B_2N_6 systems was demonstrated to be able to accurately predict the decomposition of the initial precursors, the formation of the first B−N-containing compound, and the end thermodynamically stable BN product. This model can be efficiently applied to future CFD simulations of hBN synthesis in practical devices once combined with a surface chemistry model for hBN formation, which is the direction of our future work.

■ ASSOCIATED CONTENT

Supporting Information

The Supporting Information is available free of charge at https://pubs.acs.org/doi/10.1021/acs.jpca.3c08051.

Reaction mechanism and additional simulation results including Arrhenius plots and time evolution for the major intermediate products and radicals (PDF)

https://doi.org/10.1021/acs.jpca.3c08051
J. Phys. Chem. A 2024, 128, 2584−2593

AUTHOR INFORMATION

Corresponding Author

Yuan Xuan − *Department of Mechanical Engineering, The Pennsylvania State University, University Park, Pennsylvania 16802, United States*; Email: yux19@psu.edu

Authors

Ga-Un Jeong − *Department of Mechanical Engineering, The Pennsylvania State University, University Park, Pennsylvania 16802, United States*; orcid.org/0009-0005-1417-6984

Adri C. T. van Duin − *Department of Mechanical Engineering, The Pennsylvania State University, University Park, Pennsylvania 16802, United States*; orcid.org/0000-0002-3478-4945

Complete contact information is available at: https://pubs.acs.org/10.1021/acs.jpca.3c08051

Notes

The authors declare no competing financial interest.

ACKNOWLEDGMENTS

We acknowledge the financial support from the NSF through the Penn State 2D Crystal Consortium-Materials Innovation Platform (2DCC-MIP) under DMR-1539916 and DMR-2039351.

REFERENCES

(1) Watanabe, K.; Taniguchi, T.; Kanda, H. Direct-Bandgap Properties and Evidence for Ultraviolet Lasing of Hexagonal Boron Nitride Single Crystal. *Nat. Mater.* **2004**, *3* (6), 404−409.

(2) Watanabe, K.; Taniguchi, T.; Niiyama, T.; Miya, K.; Taniguchi, M. Far-Ultraviolet Plane-Emission Handheld Device Based on Hexagonal Boron Nitride. *Nat. Photonics* **2009**, *3* (10), 591−594.

(3) Kubota, Y.; Watanabe, K.; Tsuda, O.; Taniguchi, T. Deep Ultraviolet Light-Emitting Hexagonal Boron Nitride Synthesized at Atmospheric Pressure. *Science* **2007**, *317* (5840), 932−934.

(4) Vuong, T. Q. P.; Cassabois, G.; Valvin, P.; Rousseau, E.; Summerfield, A.; Mellor, C. J.; Cho, Y.; Cheng, T. S.; Albar, J. D.; Eaves, L.; Foxon, C. T.; Beton, P. H.; Novikov, S. V.; Gil, B. Deep Ultraviolet Emission in Hexagonal Boron Nitride Grown by High-Temperature Molecular Beam Epitaxy. *2d Mater.* **2017**, *4* (2), 021023.

(5) Wang, H.; Zhao, Y.; Xie, Y.; Ma, X.; Zhang, X. Recent Progress in Synthesis of Two-Dimensional Hexagonal Boron Nitride. *J. Semicond.* **2017**, *38* (3), 031003.

(6) Ahmed, K.; Dahal, R.; Weltz, A.; Lu, J. J. Q.; Danon, Y.; Bhat, I. B. Effects of Sapphire Nitridation and Growth Temperature on the Epitaxial Growth of Hexagonal Boron Nitride on Sapphire. *Mater. Res. Express* **2017**, *4* (1), 015007.

(7) Chubarov, M.; Pedersen, H.; Högberg, H.; Czigany, Z.; Henry, A. Chemical Vapour Deposition of Epitaxial Rhombohedral BN Thin Films on SiC Substrates. *CrystEngComm* **2014**, *16* (24), 5430−5436.

(8) Chubarov, M.; Pedersen, H.; Högberg, H.; Jensen, J.; Henry, A. Growth of High Quality Epitaxial Rhombohedral Boron Nitride. *Cryst. Growth Des.* **2012**, *12* (6), 3215−3220.

(9) Chubarov, M.; Pedersen, H.; Högberg, H.; Henry, A.; Czigány, Z. Initial Stages of Growth and the Influence of Temperature during Chemical Vapor Deposition of Sp^2-BN Films. *J. Vac. Sci. Technol., A* **2015**, *33* (6), 061520.

(10) Paduano, Q.; Snure, M.; Weyburne, D.; Kiefer, A.; Siegel, G.; Hu, J. Metalorganic Chemical Vapor Deposition of Few-Layer Sp2 Bonded Boron Nitride Films. *J. Cryst. Growth* **2016**, *449*, 148−155.

(11) Rice, A.; Allerman, A.; Crawford, M.; Beechem, T.; Ohta, T.; Spataru, C.; Figiel, J.; Smith, M. Effects of Deposition Temperature and Ammonia Flow on Metal-Organic Chemical Vapor Deposition of Hexagonal Boron Nitride. *J. Cryst. Growth* **2018**, *485*, 90−95.

(12) Pierson, H. O. Boron Nitride Composites By Chemical Vapor Deposition*. *J. Compos. Mater.* **1975**, *9*, 228−240.

(13) Rozenberg, A. S.; Sinenko, Y. A.; Chukanov, N. V. Regularities of Pyrolytic Boron Nitride Coating Formation on a Graphite Matrix. *J. Mater. Sci.* **1993**, *28*, 5528−5533.

(14) Adams, A. C. Characterization of Films Formed by Pyrolysis of Borazine. *J. Electrochem. Soc.* **1981**, *128* (6), 1378−1379.

(15) Sutter, P.; Lahiri, J.; Albrecht, P.; Sutter, E. Chemical Vapor Deposition and Etching of High-Quality Monolayer Hexagonal Boron Nitride Films. *ACS Nano* **2011**, *5* (9), 7303−7309.

(16) Ćavar, E.; Westerström, R.; Mikkelsen, A.; Lundgren, E.; Vinogradov, A. S.; Ng, M. L.; Preobrajenski, A. B.; Zakharov, A. A.; Mårtensson, N. A Single H-BN Layer on Pt(1 1 1). *Surf. Sci.* **2008**, *602* (9), 1722−1726.

(17) Bao, J.; Jeppson, K.; Edwards, M.; Fu, Y.; Ye, L.; Lu, X.; Liu, J. Synthesis and Applications of Two-Dimensional Hexagonal Boron Nitride in Electronics Manufacturing. *Electron. Mater. Lett.* **2016**, *12*, 1−16.

(18) Kim, K. K.; Hsu, A.; Jia, X.; Kim, S. M.; Shi, Y.; Hofmann, M.; Nezich, D.; Rodriguez-Nieva, J. F.; Dresselhaus, M.; Palacios, T.; Kong, J. Synthesis of Monolayer Hexagonal Boron Nitride on Cu Foil Using Chemical Vapor Deposition. *Nano Lett.* **2012**, *12* (1), 161−166.

(19) Kim, G.; Jang, A. R.; Jeong, H. Y.; Lee, Z.; Kang, D. J.; Shin, H. S. Growth of High-Crystalline, Single-Layer Hexagonal Boron Nitride on Recyclable Platinum Foil. *Nano Lett.* **2013**, *13* (4), 1834−1839.

(20) Yamada, H.; Inotsume, S.; Kumagai, N.; Yamada, T.; Shimizu, M. Comparative Study of Boron Precursors for Chemical Vapor-Phase Deposition-Grown Hexagonal Boron Nitride Thin Films. *Phys. Status Solidi A* **2021**, *218* (3), 2000241.

(21) Chugh, D.; Wong-Leung, J.; Li, L.; Lysevych, M.; Tan, H. H.; Jagadish, C. Flow Modulation Epitaxy of Hexagonal Boron Nitride. *2d Mater.* **2018**, *5* (4), 045018.

(22) Mendelson, N.; Chugh, D.; Reimers, J. R.; Cheng, T. S.; Gottscholl, A.; Long, H.; Mellor, C. J.; Zettl, A.; Dyakonov, V.; Beton, P. H.; Novikov, S. V.; Jagadish, C.; Tan, H. H.; Ford, M. J.; Toth, M.; Bradac, C.; Aharonovich, I. Identifying Carbon as the Source of Visible Single-Photon Emission from Hexagonal Boron Nitride. *Nat. Mater.* **2021**, *20* (3), 321−328.

(23) Snure, M.; Paduano, Q.; Kiefer, A. Effect of Surface Nitridation on the Epitaxial Growth of Few-Layer Sp2 BN. *J. Cryst. Growth* **2016**, *436*, 16−22.

(24) Middleman, S. The Role of Gas-Phase Reactions in Boron Nitride Growth by Chemical Vapor Deposition. *Mater. Sci. Eng.* **1993**, *163*, 135−140.

(25) Yamada, H.; Inotsume, S.; Kumagai, N.; Yamada, T.; Shimizu, M. Chemical Vapor Deposition Growth of BN Thin Films Using B2H6 and NH3. *Phys. Status Solidi B* **2020**, *257* (2), 1900318.

(26) Bansal, A.; Zhang, X.; Redwing, J. M. Gas Source Chemical Vapor Deposition of Hexagonal Boron Nitride on C-Plane Sapphire Using B2H6 and NH3. *J. Mater. Res.* **2021**, *36* (23), 4678−4687.

(27) Murarka, S. P.; Chang, C. C.; Wang, D. N. K.; Smith, T. E. Effect of Growth Parameters on the CVD of Boron Nitride and Phosphorus-Doped Boron Nitride. *J. Electrochem. Soc.* **1979**, *126* (11), 1951−1957.

(28) Gomez-Aleixandre, C.; Diaz, D.; Orgaz, F.; Albella, J. M. Reaction of Diborane and Ammonia Gas Mixtures in a Chemical Vapor Deposition Hot-Wall Reactor. *J. Phys. Chem.* **1993**, *97*, 11043−11046.

(29) Gómez-Aleixandre, C.; Essafti, A.; Fernández, M.; Fierro, J. L. G.; Albella, J. M. Influence of Diborane Flow Rate on the Structure and Stability of CVD Boron Nitride Films. *J. Phys. Chem.* **1996**, *100* (6), 2148−2153.

(30) Xuan, Y.; Jain, A.; Zafar, S.; Lotfi, R.; Nayir, N.; Wang, Y.; Choudhury, T. H.; Wright, S.; Feraca, J.; Rosenbaum, L.; Redwing, J. M.; Crespi, V.; van Duin, A. C. T. Multi-Scale Modeling of Gas-Phase Reactions in Metal-Organic Chemical Vapor Deposition Growth of WSe2. *J. Cryst. Growth* **2019**, *527*, 125247.

(31) Van Duin, A. C. T.; Dasgupta, S.; Lorant, F.; Goddard, W. A. ReaxFF: A Reactive Force Field for Hydrocarbons. *J. Phys. Chem. A* **2001**, *105* (41), 9396−9409.
(32) Chenoweth, K.; Van Duin, A. C. T.; Goddard, W. A. ReaxFF Reactive Force Field for Molecular Dynamics Simulations of Hydrocarbon Oxidation. *J. Phys. Chem. A* **2008**, *112* (5), 1040−1053.
(33) Senftle, T. P.; Hong, S.; Islam, M. M.; Kylasa, S. B.; Zheng, Y.; Shin, Y. K.; Junkermeier, C.; Engel-Herbert, R.; Janik, M. J.; Aktulga, H. M.; Verstraelen, T.; Grama, A.; Van Duin, A. C. T. The ReaxFF Reactive Force-Field: Development, Applications and Future Directions. *npj Comput. Mater.* **2016**, *2*, 15011.
(34) Lele, A.; Krstic, P.; Van Duin, A. C. T. ReaxFF Force Field Development for Gas-Phase HBN Nanostructure Synthesis. *J. Phys. Chem. A* **2022**, *126* (4), 568−582.
(35) Kwon, H.; Lele, A.; Zhu, J.; McEnally, C. S.; Pfefferle, L. D.; Xuan, Y.; van Duin, A. C. T. ReaxFF-Based Molecular Dynamics Study of Bio-Derived Polycyclic Alkanes as Potential Alternative Jet Fuels. *Fuel* **2020**, *279*, 118548.
(36) Lele, A.; Kwon, H.; Ganeshan, K.; Xuan, Y.; van Duin, A. C. T. ReaxFF Molecular Dynamics Study on Pyrolysis of Bicyclic Compounds for Aviation Fuel. *Fuel* **2021**, *297*, 120724.
(37) Döntgen, M.; Przybylski-Freund, M. D.; Kröger, L. C.; Kopp, W. A.; Ismail, A. E.; Leonhard, K. Automated Discovery of Reaction Pathways, Rate Constants, and Transition States Using Reactive Molecular Dynamics Simulations. *J. Chem. Theory Comput.* **2015**, *11* (6), 2517−2524.
(38) Kee, R. J.; Rupley, F. M.; Miller, J. A.; Coltrin, M. E.; Grcar, J. F.; Meeks, E.; Moffat, H. K.; Lutz, A. E.; Dixon Lewis, G.; Smooke, M. D.; Warnatz, J.; Evans, G. H.; Larson, R. S.; Mitchell, R. E.; Petzold, L. R.; Reynolds, W. C.; Caracotsios, M.; Stewart, W. E.; Glarborg, P. *Chemkin Collection*. Release 3.5,; Reaction Design, Inc.: San Diego, CA. USA, 1999.
(39) Karalus, M. F.; Fackler, K. B.; Novosselov, I. V.; Kramlich, J. C.; Malte, P. C. A Skeletal Mechanism for the Reactive Flow Simulation of Methane Combustion *Proceedings of the ASME Turbo Expo 2013: Turbine Technical Conference and Exposition. Vol. 1B: Combustion, Fuels and Emissions*: San Antonio, Texas, USA, 2013..
(40) Glarborg, P. The NH3/NO2/O2 System: Constraining Key Steps in Ammonia Ignition and N2O Formation. *Combust. Flame* **2023**, *257*, 112311.
(41) Krstic, P. S.; Han, L.; Irle, S.; Nakai, H. Simulations of the Synthesis of Boron-Nitride Nanostructures in a Hot, High Pressure Gas Volume. *Chem. Sci.* **2018**, *9* (15), 3803−3819.

https://doi.org/10.1021/acs.jpca.3c08051
J. Phys. Chem. A 2024, 128, 2584−2593